

## Supporting Materials

# Enhanced efficiency of water desalination in nanostructured thin-film membranes with polymer grafted nanoparticles

Aparna Swain<sup>1,†</sup>, S Adarsh<sup>1,†</sup>, Ashish Biswas<sup>1,†</sup>, Suryasarathi Bose<sup>2,‡</sup>, Brian C. Benicewicz<sup>3,¶</sup>, Sanat K. Kumar<sup>4,\*.§</sup> and J. K. Basu<sup>1\*,†</sup>

<sup>†</sup>*Department of Physics, Indian Institute of Science Bangalore, 560012, India*

<sup>‡</sup>*Department of Materials Engineering, Indian Institute of Science Bangalore, 560012, India*

<sup>¶</sup>*Department of Chemical Engineering, University of South Carolina, Columbia, South Carolina, USA*

<sup>§</sup>*Department of Chemical Engineering, Columbia University, 10027, New York, USA*

E-mail: sk2794@columbia.edu; basu@iisc.ac.in

This supporting document includes information on sample preparation, characterization of polymer grafted nanoparticle (PGNP) membranes and substrates, and information on measurement techniques such as atomic force microscopy, scanning electron microscopy and transmission electron microscopy etc., which were utilized to investigate the evolution of surface morphology of modified PGNP based polyamide - thin film composite (PA-TFC) membranes.

## Sample preparation and characterization

PMA-g-SiO<sub>2</sub> samples were prepared using SI-RAFT technique.<sup>1</sup> Commercial PA-TFC membranes were modified chemically using 87% v/v DMF solution.<sup>2</sup> PGNP monolayers were transferred on the substrate by Langmuir-Schaefer (LS) method. PGNP multi-layers were made by layer-by-layer deposition using LS technique.

### Sample preparation

All experiments are carried out on ultra-thin layer of polymethylacrylate (PMA) grafted gold nanoparticles (PGNPs) transferred onto modified PA-TFC membranes. PMA grafted spherical silica particles (PMA-g-SiO<sub>2</sub>) were synthesized by the surface initiated reversible addition-fragmentation chain transfer polymerization (SI-RAFT) technique.<sup>1</sup> Here, the RAFT agent 2-(dodecylthiocarbonothioylthio) propanoic acid (DoPAT) was used for the polymerization. All chemicals were obtained from either Fisher or Acros and used as received unless otherwise specified. Colloidal silica nanoparticles (13±1 nm diameter) were obtained from Nissan Chemical. 3-aminopropyldimethylethoxysilane was purchased from Gelest, Inc. and used as received. DoPAT was purchased from Boron Molecular, Inc. Methyl acrylate (MA, 99, Acros) was purified by passing through an activated basic alumina column. Azobisisobutyronitrile (AIBN) was recrystallized from ethanol twice before use. <sup>1</sup>H NMR and <sup>13</sup>C NMR (Bruker Avance 300) were conducted using CDCl<sub>3</sub> as solvent. Molecular weights and dispersities were determined using a gel permeation chromatograph (GPC) equipped with a Varian 290-LC pump, a Varian 390-LC refractive index detector, and three Styragel columns (HR1, HR3 and HR4, molecular weight of 29000, 88000, and 132000, respectively). Tetrahydrofuran (THF) was used as eluent for the GPC at 30°C and a flow rate of 1.0 mL/min. The GPC was calibrated with Poly(methyl acrylate) (PMA) standards obtained from Polymer Laboratories. Synthesized particles are dried under vacuum to remove any traces of the solvent. They are further characterized through a palette of techniques to measure their

overall size, core size, density of grafted polymers, and the glass transition temperature of the respective membranes. PGNPs are characterized using transmission electron microscopy (TEM), thermo gravimetric analysis (TGA) and small angle X-ray scattering (SAXS) (Fig. S1(a) and (b)). The effective NP core diameter is deduced from TEM. TEM images of PGNPs with graft chain molecular weight  $M_w = (29 \text{ kDa}), (88\text{kDa})$  and  $(132 \text{ kDa})$  have been provided in Fig. S1(c)-(e). The size distribution histograms of the effective diameter of the respective PGNPs are shown inside the corresponding images.

## Characterization of PGNPs

We have used SAXS (Bruker, Nanostar Germany) to measure the overall PGNP size, combining both the core and the grafted PMA shell. SAXS intensity ( $I$ ) vs wave vector ( $Q$ ) profiles of melt samples of different PGNPs, shown in ( Fig. S1(a)) capture the structure factor peak characterizing the mean separation between two neighboring PGNPs, which is equivalent to the diameter of the PGNP in melt. TGA (Fig. S1) (b) was performed to get the mean weight fraction of the silica nanoparticle core and PMA corona in the PGNPs. The grafting density,  $\sigma$ , of the PGNPs used was estimated using silica fraction from the TGA and core diameter obtained from TEM (shown in Fig. S1 (c)-(e)). We have extracted the diameter of the silica particles from the TEM images, where we show the corresponding diameter distributions in Fig. S1 (f)-(i).

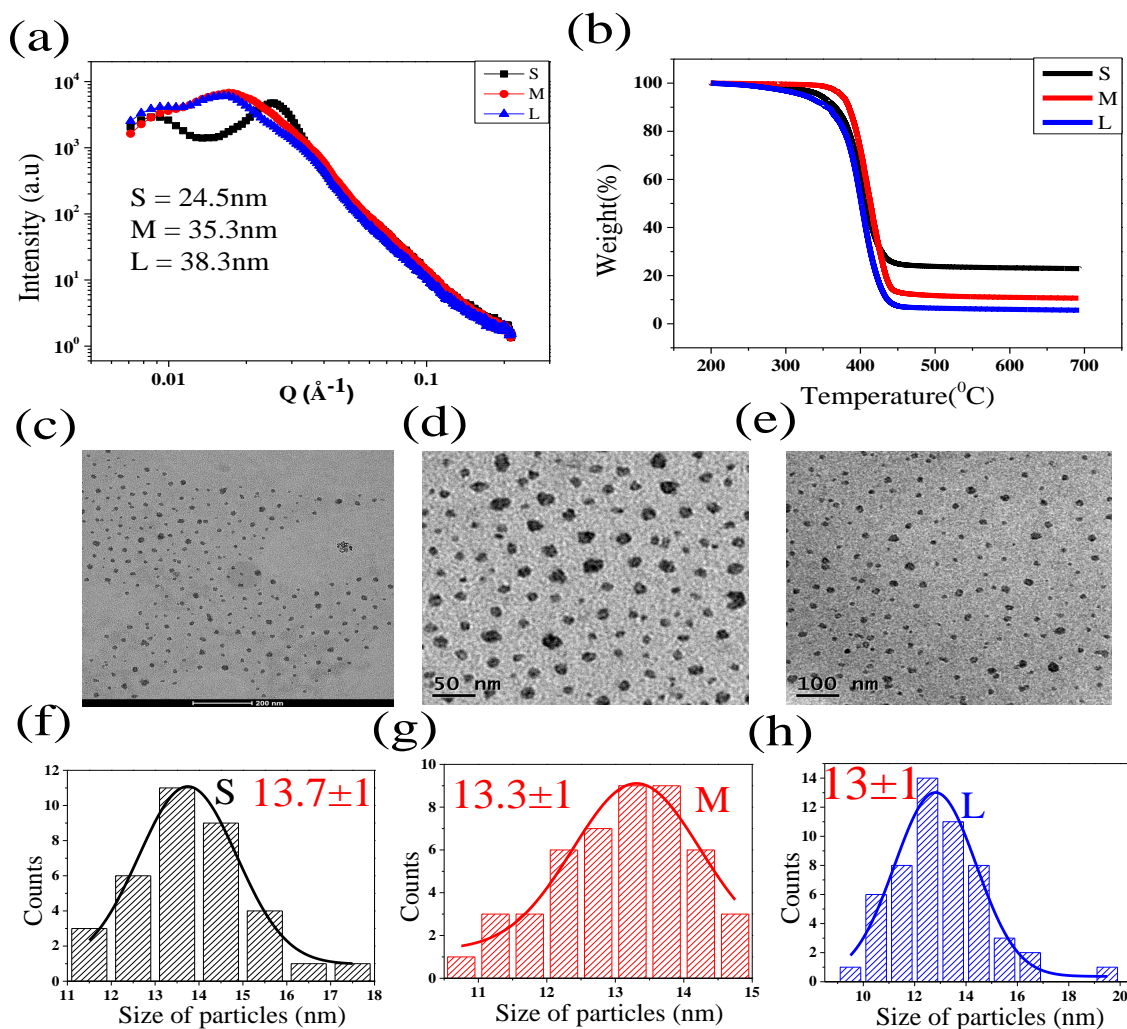


Fig. S1: a) SAXS intensity  $I$ , vs wavevector,  $Q$ , data for PGNP-S, PGNP-M and PGNP-L samples in melt state. b) TGA data of all the PGNP samples. TEM images of PGNPs of type (c) S, (d) M and (e) L. The corresponding distribution of diameters of the (f) S, (g) M and (h) L PGNP, respectively.

## Modification of the membrane using chemical treatment

In this work, we employ pore structure re-construction to decrease the operating pressure from 75 psi to a lower value. A support surface pore structure re-construction method was developed to enhance the flux of the thin film composite (TFC) reverse osmosis (RO) membranes. An aqueous solution of a suitable organic solvent with specific solvent content, i.e., re-construction agent, was used to swell the support for a period of time and then

the swelled support was immersed in water to deswell and complete the whole surface pore structure re-construction process. Herein, dimethylformamide (DMF) was utilized as the organic solvent. Under proper conditions (i.e., the organic solvent content of 87 % v/v, a re-constructing agent contacting time of less than 30 s and re-constructing agent contacting temperature of  $25\pm 2$  °C) in the sonication bath, it was found that the support surface porosity and pore density values increased along with a slight increase in the support surface pore size. In Fig. S2 (a) and (b) shows SEM images for the front and back surface of pristine PA membrane while in Fig. S2 (c) and (d) the same is shown after the modification of the membrane. In Fig. S2(d) , the nanopores formed after the compaction.

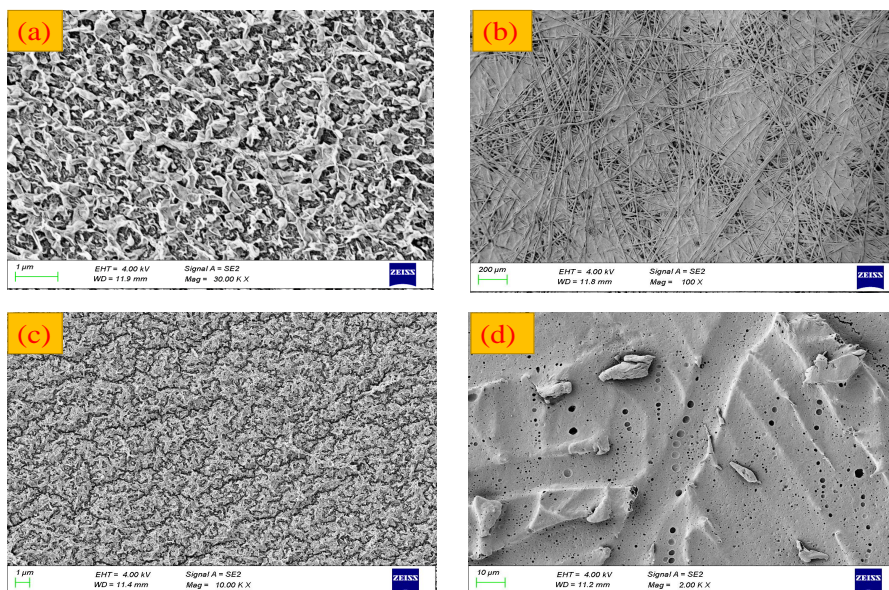


Fig. S2: SEM images of the pristine PA membrane corresponding to (a) front side and (b) backside. Same for the modified PA membrane showing (c) the front side and (d) the backside. The enhanced porosity for modified PA membranes compared to the pristine ones is clearly visible

To clearly distinguish the support surface pore structure, threshold images for SEM surface images were analyzed by using ImageJ software (National Institute of Health, <http://rsb.info.nih.gov/ij>) according to the procedure described in.<sup>3</sup> The nanopores can be clearly seen from the threshold images (small black dots) in Fig. S3.

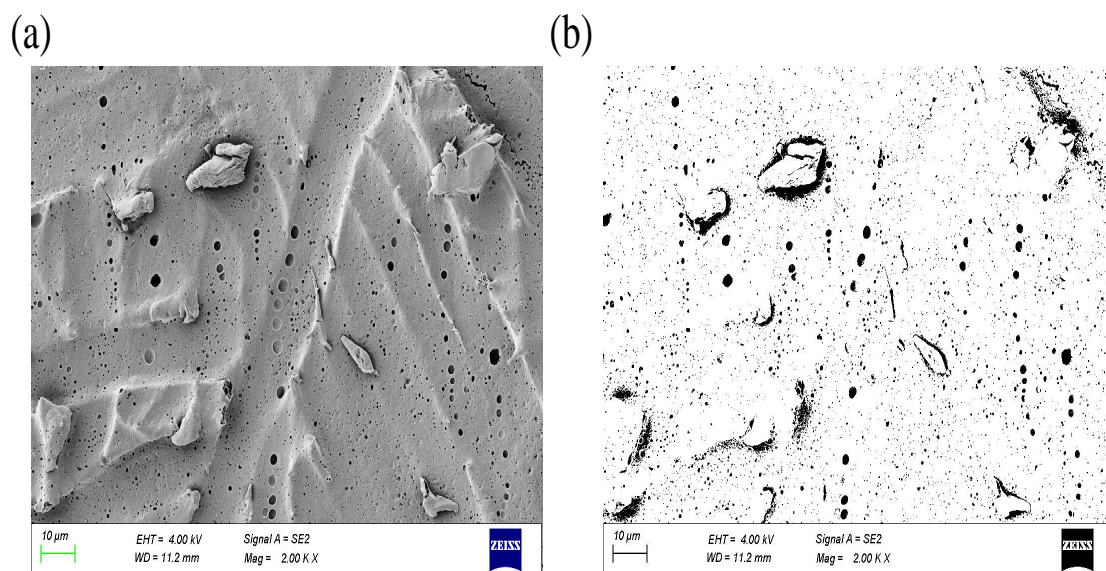


Fig. S3: (a) SEM images of the backside and (b) the threshold images of modified PA membrane.

### PGNP compact monolayer formation by using LB method:-

The pristine PA membrane of a larger size of dimension (35cm x 50cm) is shown in Fig. S4 (a). We have taken one small portion of the membrane for the modification. Then after that, we used the transfer of the PGNP layer on top of the modified membrane is shown in Fig. S4 (b) of the area of the through  $155\text{cm}^2$ . A monolayer of PGNP was created at the air/water interface in a Langmuir–Blodgett (LB) trough (KSV NIMA, Finland) using the following procedure. Approximately  $400\ \mu\text{l}$  of a homogeneous solution of PGNPs (0.75 g/l) in toluene was spread on the water surface using a Hamilton syringe. A monolayer of connected of PGNPs was formed upon the evaporation of the solvent. A dense membrane of PGNPs with thickness ranging from 25-40 nm depending on  $M_n$  was obtained by compressing the mesoscopic ordered structures of the PGNPs to a surface pressure of  $\Pi = 35\ \text{mN/m}$  or  $37\ \text{mN/m}$ . The isotherm curves for  $M_n = 29\ \text{KDa}$ ,  $88\ \text{KDa}$ , and  $132\ \text{KDa}$  are shown in Fig. S5. The ability to follow the changes in surface pressure during compression allowed us to measure the isothermal compression modulus.

$$\kappa_f = -A_M \frac{\partial \Pi}{\partial A_M} \Big|_T, \quad (1)$$

where  $A_M$  is the total available area in between the limiting mechanical barriers used to compress the monolayers and  $T$  is the temperature. Compression modulus of membranes at the final transfer pressure 35 mN/m,  $\kappa_f$  (given in Table 1 in main manuscript) is a signature of the softness, or equivalently flexibility, of these membranes. However, intriguingly the flexibility ( $\kappa_f$ ) of the membranes depend non-monotonically on the graft molecular weight of the individual PGNPs, labeled as S, M, L, respectively (Table 1 in main manuscript).

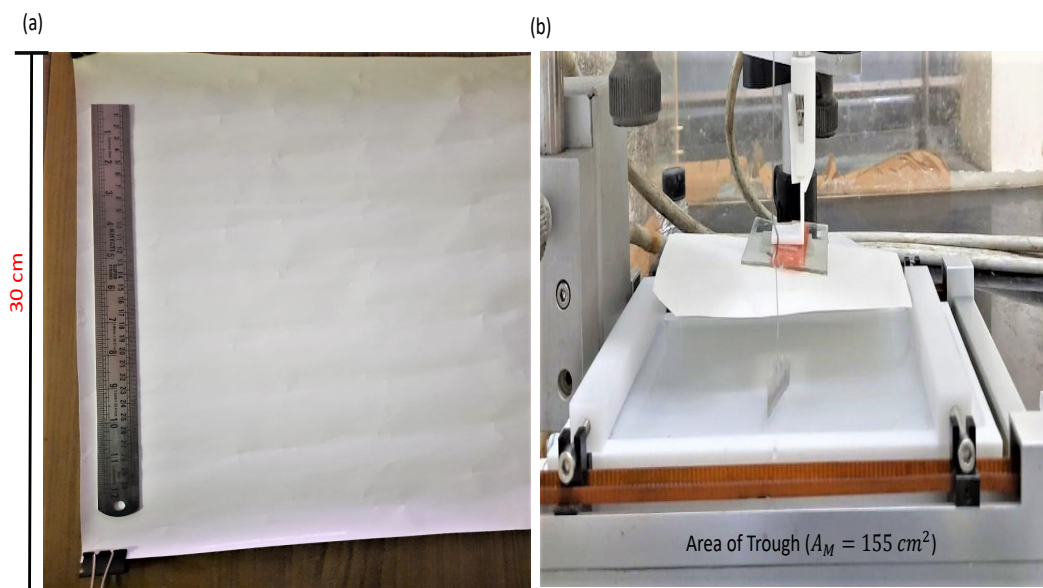


Fig. S4: (a) The size of the Pristine PA membrane. The length scale has mentioned in the figure. (b) The photo of the Langmuir- Schaefer(LS) method while transferring the PGNPs of monolayers at a sub-phase (water) temperature of 25<sup>0</sup>C of trough area 150 cm<sup>2</sup>.

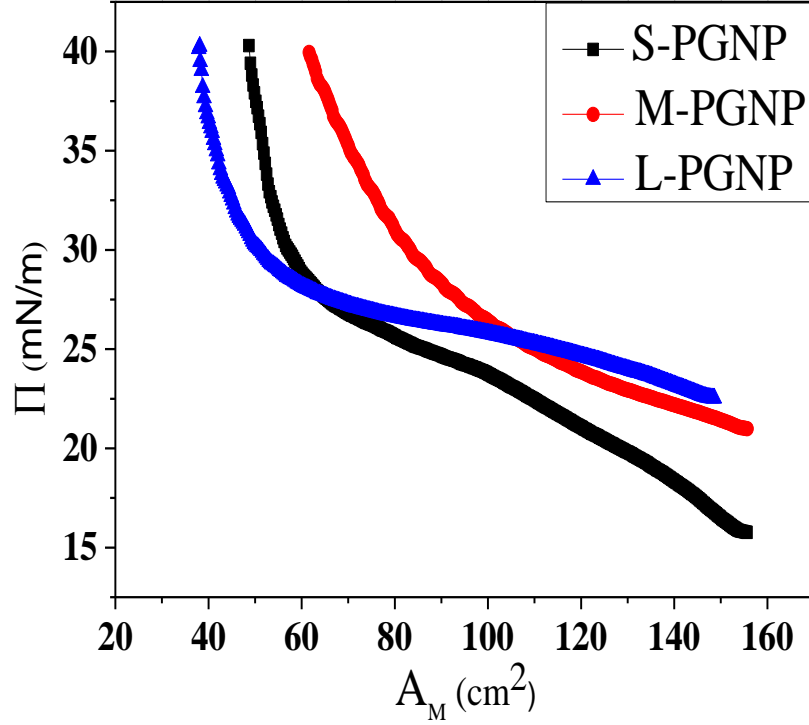


Fig. S5: Langmuir isotherms ( $\Pi$  vs  $A_M$ ) for S-PGNP, M-PGNP and L-PGNP monolayers at a subphase (water) temperature of 25°C.

The modified TFC nanocomposite membranes were prepared in a two-step process.<sup>4</sup> In the first step, the pristine PA membrane was modified by chemical treatment. The treatment process was described elaborately in the previous section. In the second step, PGNP membranes were prepared at the air/water interface in a Langmuir trough.<sup>4-6</sup> The monolayer formed was then transferred on top of the modified membrane to complete the process. The PGNP layer is very compact as we can see from SEM images shown in Fig. S6(a)-(c).

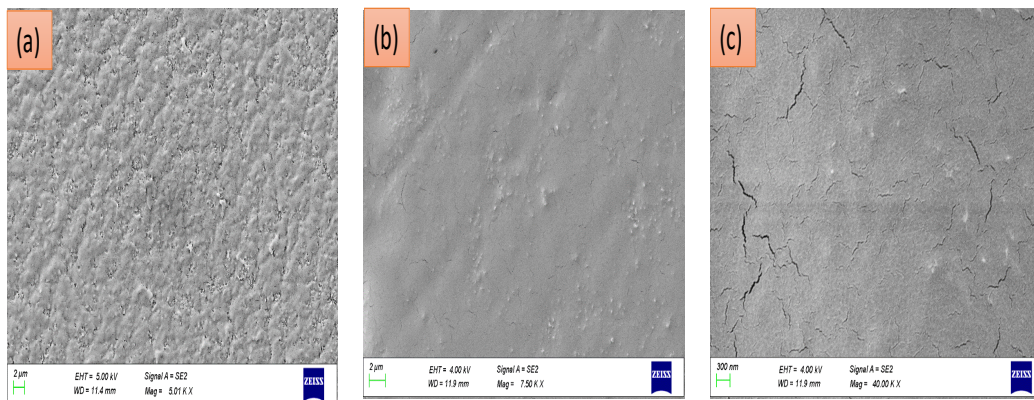
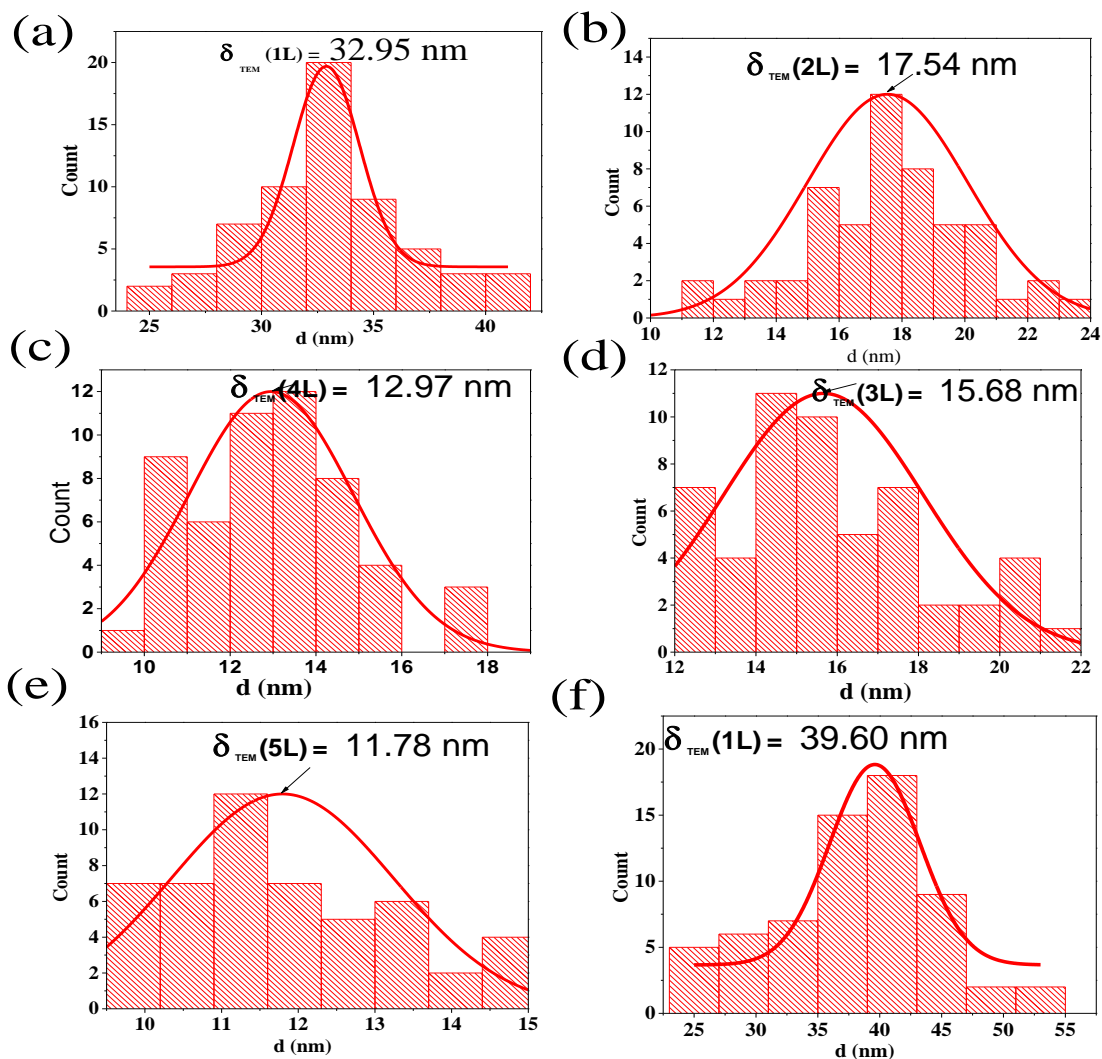


Fig. S6: SEM images of the layered transferred on modified PA membranes for (a)  $N = 1$  layer of M-PGNPs, (b)  $N = 3$  layers of M-PGNPs and (c)  $N = 5$  layers of L-PGNPs transferred on modified PA membranes.

We repeated the second step for making multilayer samples. The number of layers were increased by the layer-by-layer deposition of PGNP membranes by the LB method. The inter-particle distance between PGNPs decreased when the number of layers was increased, Fig. ((a)-(f)). In Fig. , (a) to (e) are for one to five layers transferred on TEM grids for M-PGNPs. In Fig. , (f) is for one layer of L-PGNPs.



layers M-PGNP, (e)  $N = 5$  layers M-PGNP and (f)  $N = 1$  layer of L-PGNP.  
 layers M-PGNP, (e)  $N = 5$  layers M-PGNP and (f)  $N = 1$  layer of L-PGNP.

Fig. S7: Apparent inter-particle distance,  $\delta_{TEM}$ , histograms of transferred PGNP layers on TEM grids. (a)  $N = 1$  layer M-PGNP, (b)  $N = 2$  layers M-PGNP, (c)  $N = 4$  layers M-PGNP, (d)  $N = 3$  layers M-PGNP, (e)  $N = 5$  layers M-PGNP and (f)  $N = 1$  layer of L-PGNP.

## Desalination of membrane

The operating pressure for the pristine PA membrane is 75 psi. It is difficult to get permeate below this pressure without the chemical method of pore reconstruction. We have shown the Flux and salt rejection histograms for the pristine PA membrane in Fig. S8 using the Eqn.

2 and 4. The Water permselectivity (A/B) is shown in Fig. S9. These values are below the upper bound curve.

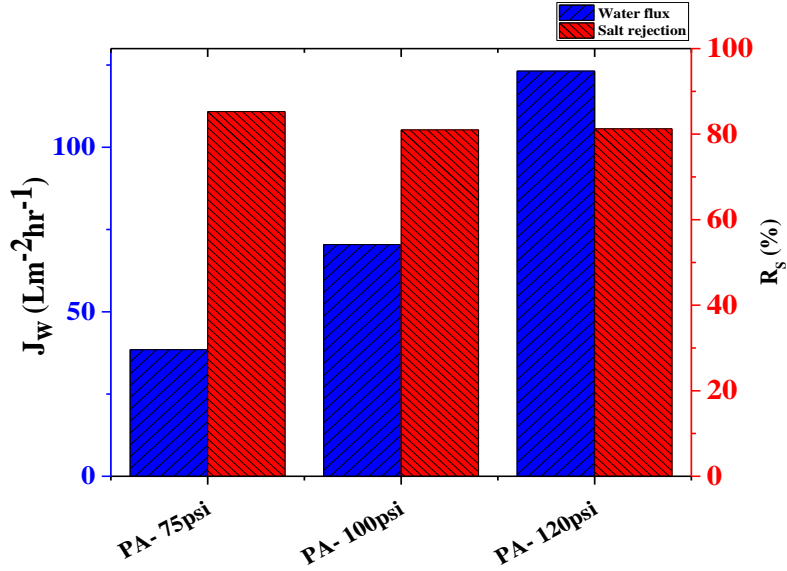


Fig. S8: Water flux,  $J_w$  and salt rejection,  $R_s$ , of the pristine PA membranes at different input pressures.

The transmembrane water flux,  $J_w$  is calculated as the volume of permeate,  $V_p$  collected across unit area of the membrane,  $a$  in unit time,  $t$ .

$$J_w[Lm^2hr^{-1}] = \frac{V_p}{a \times t} \quad (2)$$

where the area of the membrane is calculated as  $a = 2.44 \text{ cm}^2$ .

The salt flux,  $J_s$  is calculated using the volume of solute,  $V_s$  permeated across a unit area of the membrane,  $a$  in unit time,  $t$ .

$$J_s[Lm^2hr^{-1}] = \frac{V_s}{a \times t} \quad (3)$$

Here,  $V_s$  is determined by the following equation

$$V_s = V_p \times C_p \quad (4)$$

where  $C_p$  is the concentration of the permeate and  $\rho_{salt}$  is the density of salt (2.17 g/cc) in the downstream side.

The salt rejection,  $R_S$  is determined using the equation

$$R_S = \left(1 - \frac{C_p}{C_f}\right) \times 100 \quad (5)$$

where  $C_p$  and  $C_f$  are the salinity of the permeate and feed solutions.

The water permeance,  $A$  and the salt permeability,  $B$  are both determined from the relations between flux and permeance as

$$J_w = A(\Delta P - \Delta\pi) \quad J_s = B\Delta C \quad (6)$$

$$\implies A[Lm^2hr^{-1}bar^{-1}] = \frac{J_w}{(\Delta P - \Delta\pi)} \quad B[Lm^2hr^{-1}] = \frac{J_s}{\Delta C} \quad (7)$$

Here,  $\Delta P$  is the applied pressure on the membrane during the flux experiment,  $\Delta C$  is the difference between  $C_f$  and  $C_p$ , and  $\Delta\pi$  is the osmotic pressure difference where the osmotic pressure,  $\pi$  is defined as  $\pi = iMRT$ . Here,  $i$  is the van't Hoff factor,  $M$  is the molarity of the solution,  $R$  is the ideal gas constant and  $T$  is the absolute temperature.

Finally, we determine the water permselectivity of the membrane as  $A/B$ .

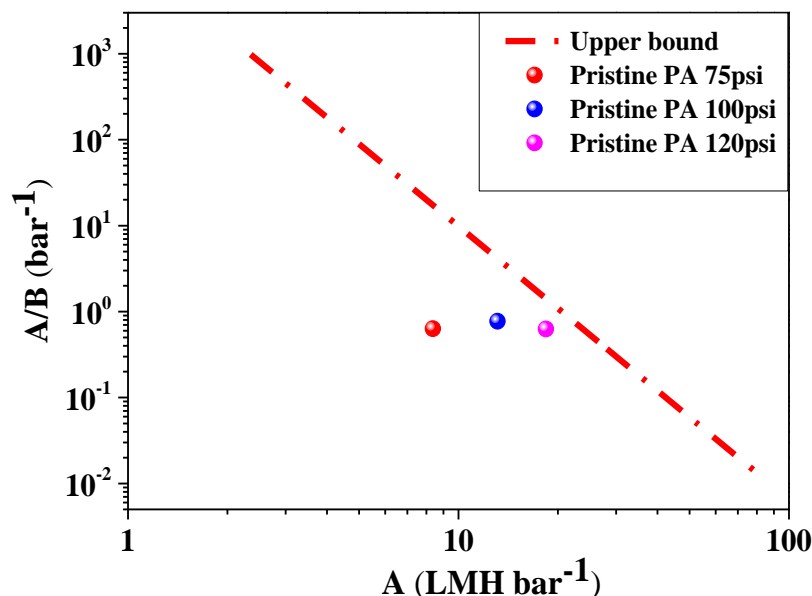


Fig. S9: The permselectivity ( $A/B$ ) vs water permeance ( $A$ ) data for the pristine PA membranes for different input pressures along with the recent upper bound (UB) curve.

## Stabilization of membranes

The modified PA membrane after the pore reconstruction chemical method<sup>2</sup> was stabilized using water before taking the measurements with saline water. Membranes when under applied pressure, common for ultrafiltration membranes, could result in a decrease of flux due to compaction and this might interfere with the appropriate analysis of support surface pore structure.<sup>7</sup> To investigate this influence, the membranes were first subjected to deionized (DI) water maintained at a pressure of 4.13 bar for an hour using the cross-flow setup. The fluxes of all the membranes decreased initially but were eventually found not to decrease significantly with time toward the end of the stabilization period. All desalination experiments were carried out with membranes only after attaining such a period of minimal variation of  $J_w$  with time. A similar procedure was followed for the stabilization of all the PGNP based modified PA membranes.

After the stabilization of membranes, the desalination experiments with saline solution corresponding to brackish water (2000 ppm) were performed at a pressure of 60 psi. Fig.

S10 (a) shows  $J_w$  and  $R_S$  histograms of modified PA membrane. A clear increase in  $J_w$  can be seen compared to a pristine PA membrane where no significant volume of permeate could be collected in any reasonable amount of time. However,  $R_S$  had also expectedly reduced. Slight variations in  $J_w$  and  $R_S$  values can be observed between membranes due to variations in processing conditions. However, the  $A/B$  and  $A$  values are very similar for all the modified membranes as shown in Fig. S10 (b).

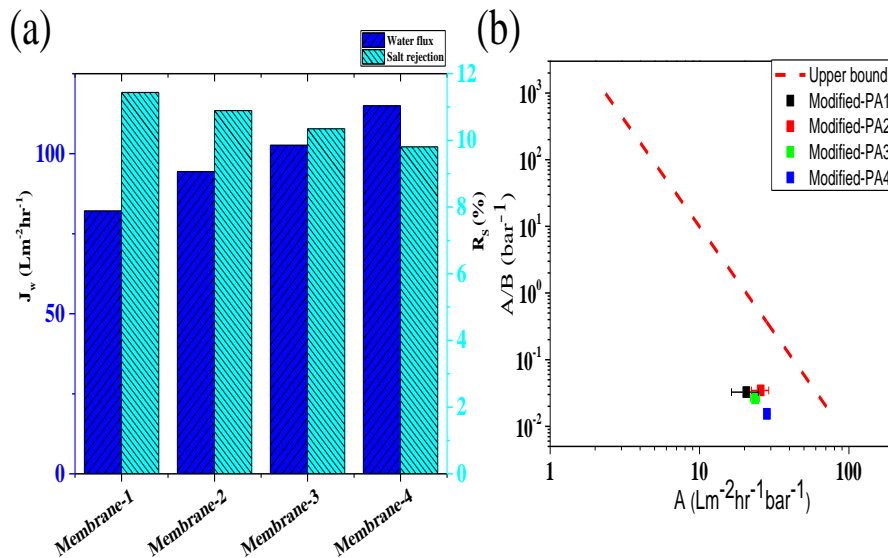


Fig. S10:  $J_w$  and  $R_S$  and the permselectivity of the modified PA membranes. (a) Water flux,  $J_w$ , and salt rejection,  $R_S$ , histograms, and (b) Permselectivity,  $A/B$  vs  $A$  for some typical modified PA-TFC membranes along with the UB curve.

In order to enhance the separation performance of the modified membranes while maintaining acceptable water flux, PGNP monolayers with various  $M_n$  values were transferred layer-by-layer using the LB technique on top of modified PA membranes. In Fig. S11 the water flux and salt rejection histograms are shown for some PGNP-based PA-TFC membranes for various values of  $N$  and  $M_n$  along with typical data for a modified PA-membrane without any PGNP layer transferred onto it. Adding PGNP layers, irrespective of  $M_n$ , leads to a decrease in  $J_w$  and an increase in  $R_S$  as compared to just the modified PA membrane. Further, we also show in Fig. S11 (b)  $J_w$  and  $R_S$  histograms for two independent membranes

with  $N = 5$  layers of M-PA indicating fairly good reproducibility of desalination efficiency of these membranes. This is also typical for other membrane systems as well. Finally, we also test the durability and long time stability of these membranes against recycling. As Fig. S11 (c) shows the  $N$  dependence for M-PA Membranes in  $J_w$  and  $R_S$  histograms. Here we see the rejection enhancement after adding the PGNP layer. Moreover, the  $J_w$  and  $R_S$  for M-PA  $N = 5$  membranes are shown in Fig. S11 (d) for the performance with time evolution.

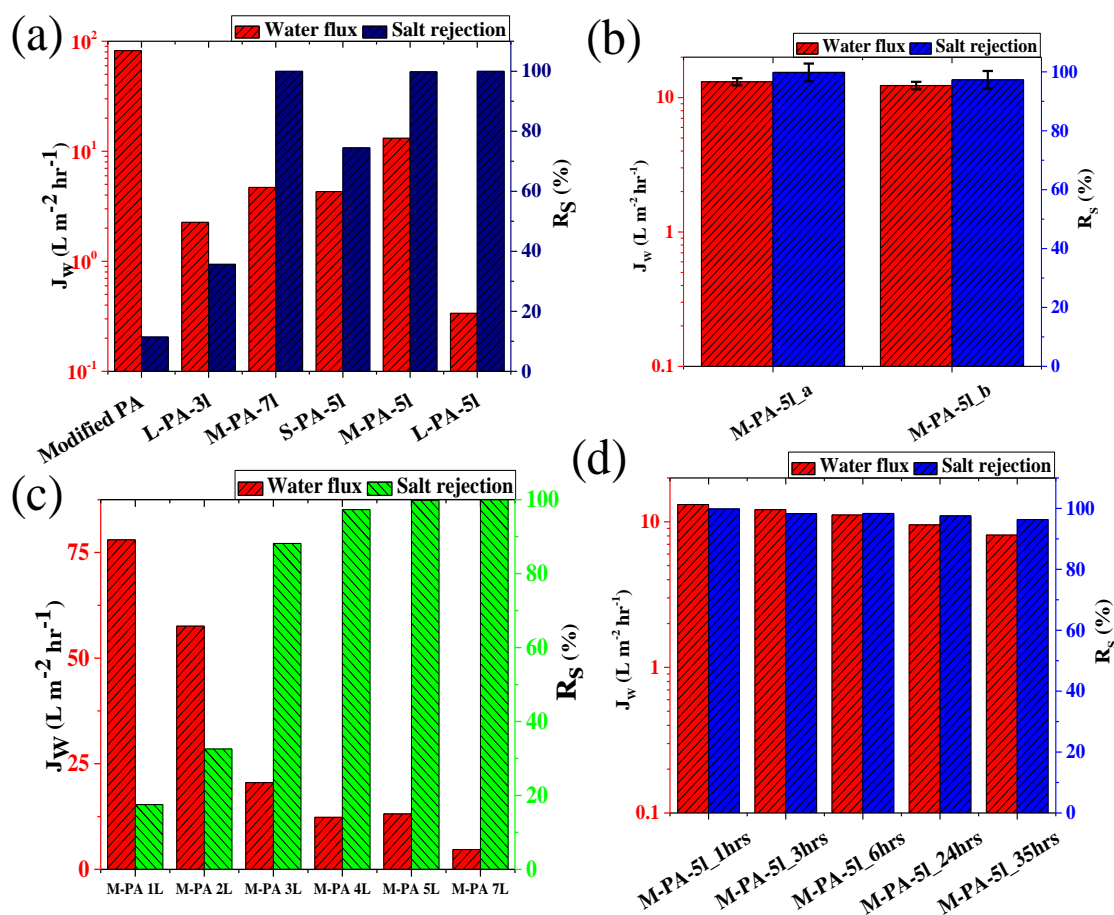


Fig. S11: (a) Water flux and Rejection of S-PA, M-PA, and L-PA membranes with various numbers of layers of PGNPs transferred on them along with similar data for a modified PA membrane without PGNP layers transferred. A general trend of decreasing  $J_w$  and increasing  $R_S$  with added PGNP layers can be clearly seen. (b)  $J_w$  and  $R_S$  for some typical M-PA  $N = 5$  membranes showing the reproducibility of the results, (c)  $N$  dependence for M-PA Membranes, and (d)  $J_w$  and  $R_S$  for M-PA  $N = 5$  membranes showing the performance with time evolution.

## Surface pressure dependence of water Perm-selectivity of PA-TFC membranes

We also observed that the membrane separation showed a dependence on the transfer surface pressure of the monolayers. In Fig. S12 we can see the effect of PGNP layer transfer  $\Pi$  dependence on both  $A/B$  and  $A$ . Here, again the M-based membranes for both  $N = 4$  and 5 showed improved separation performance with higher  $A/B$  values at  $\Pi = 37$  mN/m compared to that at 35 mN/m. Conversely, L type membranes with  $N = 4$  did not show much sensitivity to  $\Pi$ . Moreover, S based membrane with  $N= 5$  did not show much-improved separation performance with an increase in  $\Pi$  and recorded a decreased value for permeance.

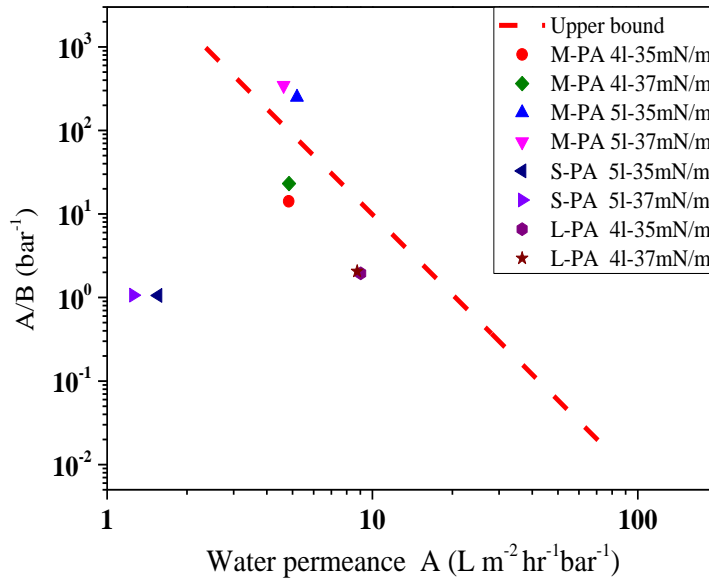


Fig. S12: Water perm-selectivity ( $A/B$ ) of all the PGNP based modified PA-TFC membranes for two different values of transfer  $\Pi$  corresponding to 35 and 37 mN/m. Only M based membranes show improved separation performance.

## Molecular weight dependence of water permeance ( $A$ ) and Salt permeability ( $B$ ) of TFC PA membranes

The PGNP layer ( $N$ ) dependence of L-PGNP based membranes is shown in Fig. S13 (a). As is clearly evident,  $J_w$  reduces and  $R_S$  increases with increasing  $N$ . Furthermore, from

Fig. S13(b), we can also clearly see the effect of  $M_n$  on  $J_w$  and  $R_S$ . Interestingly  $J_w$  is the maximum for the intermediate molecular weight graft chain, M while at the same time having  $R_S$  value which is close to the maximum.

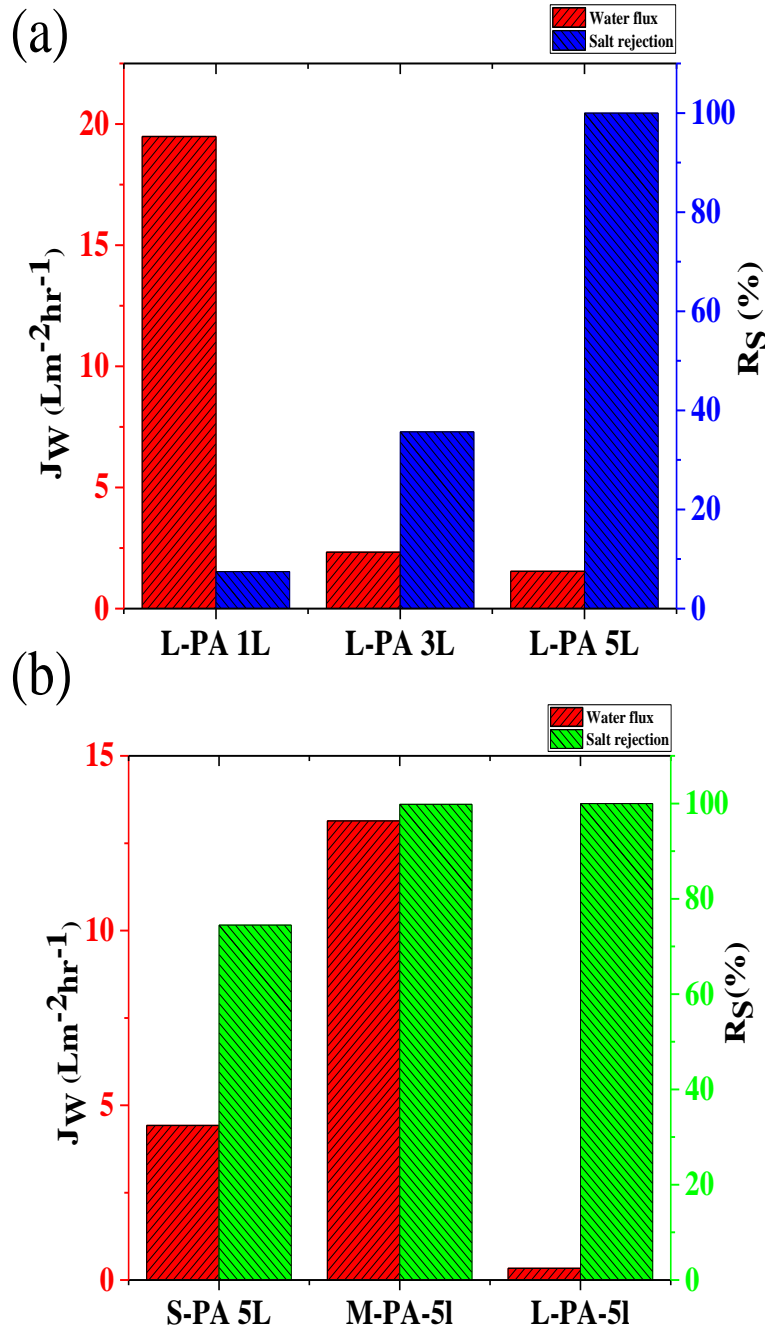


Fig. S13: (a)  $N$  dependence for L-PA Membranes. (b)  $J_w$  and  $R_S$  for S-PA, M-PA and L-PA membrane with  $N = 5$  PGNP layers.

The flux data presented in Fig. S13(b) can be further quantified in terms of the  $M_n$  dependence of  $A$  and  $B$ . Fig. S14 reflects this interesting non-monotonic dependence of  $A$  with  $M_n$ . However, the salt permeability  $B$  data, presented in Fig. S15, shows monotonic decrease with increasing  $M_n$ .

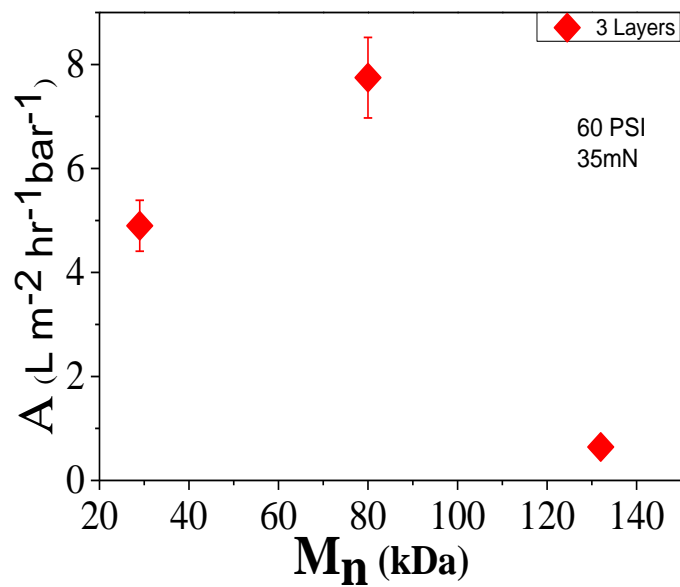


Fig. S14: Molecular weight dependence of water permeance ( $A$ ) of three layers of the modified PA-TFC membranes.

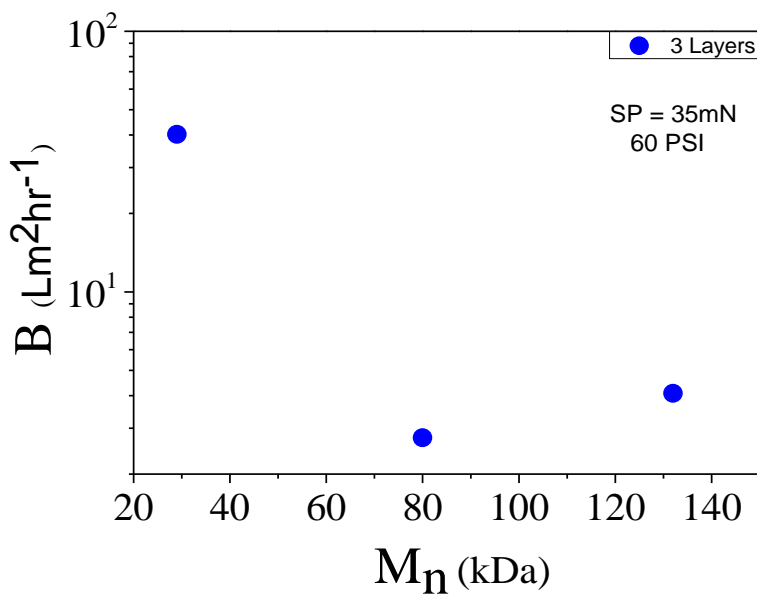


Fig. S15: Molecular weight dependence salt permeability ( $B$ ) of three layers of the modified PA-TFC membranes.

### Stability of the membranes

To see the morphology of membranes after salt rejection and running at high pressure, we have taken SEM images of membranes. In fig. S16 we show the SEM images of membranes after running the flux experiments after 35 hours indicating that they are reasonably stable after running at higher surface pressure. We checked the stability of the membrane by running the salt rejection process for 7 days. This membrane maintains a high and stable NaCl rejection at around 99% and 90% for 7 days, respectively. These results demonstrate that our membranes exhibit both good effectiveness and stability in the selective separation of NaCl from water. In Fig. S17, we also show the comparison plot of the desalination performance of some M-PA membranes having different PGNP layers when these were run continuously for up to 7 days. We notice that for the M-PA  $N = 4$  membrane rejection comes down considerably after 7 days of continuous usage while the drop in corresponding membranes with  $N = 5$  and above is less significant. We have shown the optical images of M-PA 4L and 5L in Fig. S19. The M-PA 5L looks smoother than MPA 4L. This could be

the reason for the rejection comes down considerably after 7 days.

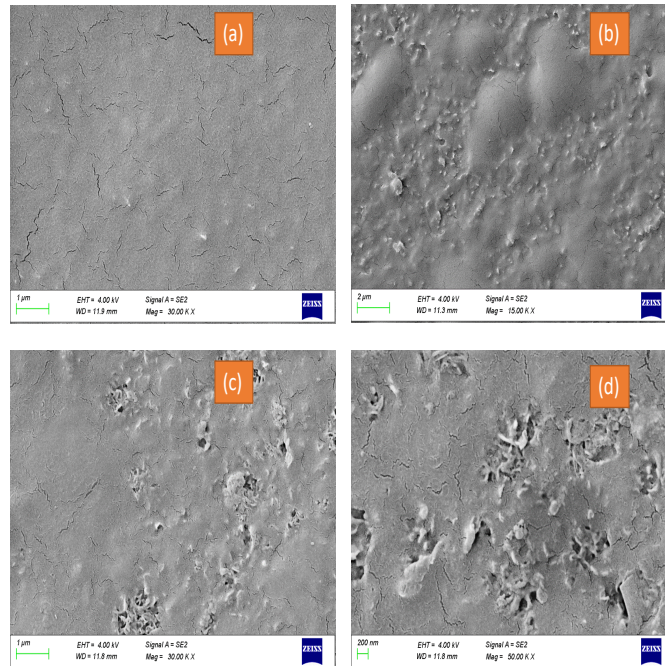


Fig. S16: SEM images of  $N = 5$  layers of M-PA-5L (a) before and (b-d) after running the flux experiment for 35 hours at three different places of the membrane.

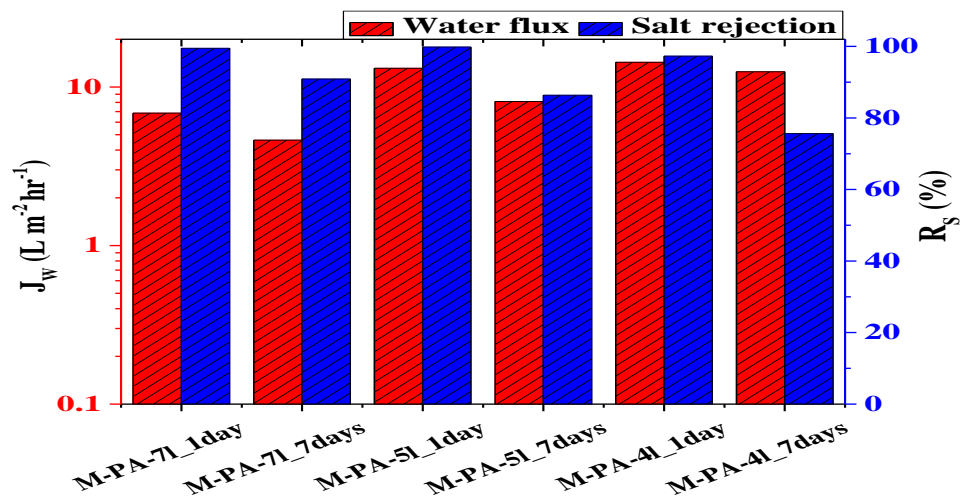


Fig. S17: The comparison plot of  $J_w$  and  $R_s$  for M-PA  $N = 7, 5,$  and  $4$  membranes showing the performance with time evolution for 7 days continuous running the experiment for the stability checking.

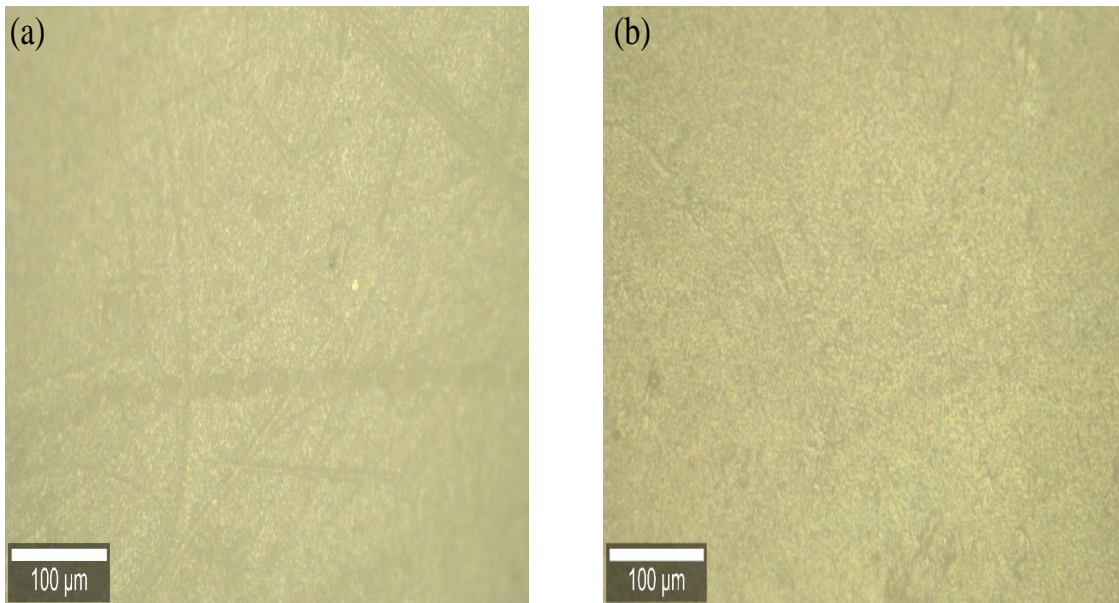
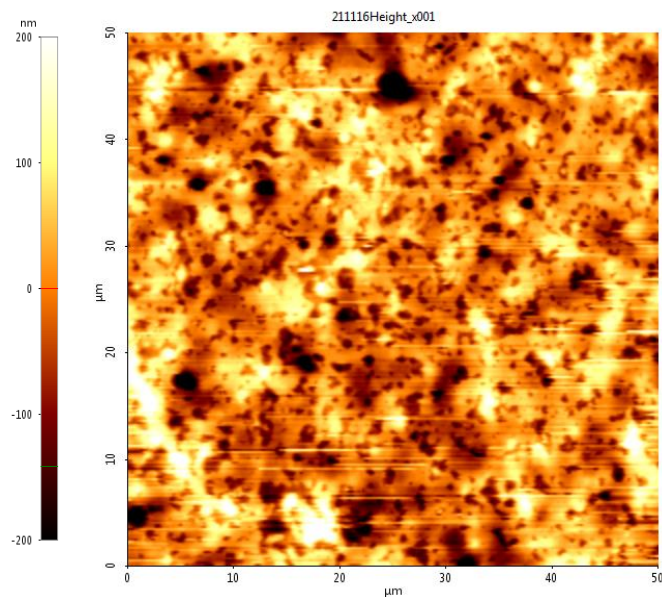


Fig. S18: (a) Optical images of (a)  $N = 4$  and (b)  $N = 5$  M-PGNP layers transferred on modified PA.

### **Morphology, water flux and salt rejection of pure polymer layers transferred on modified PA membrane**

Finally, to understand the role of chain grafting, we investigated the morphology and desalination performance of the pristine polymer monolayers as compared to those from silica nanoparticles grafted with the same polymers. For this purpose, we first studied the morphology of  $N = 5$  layers of M-PMA transferred on silicon substrate and compared it with  $N = 5$  layers of M-PGNP as shown in the AFM images in Fig. S19. From this figure, we can notice the pinholes present in the M-PMA transferred layers Fig. S19 (a), unlike for M-PGNP (Fig. S19(b)).

(a) 5L- Pristine M-Polymer



(b) 5L-M-PGNP

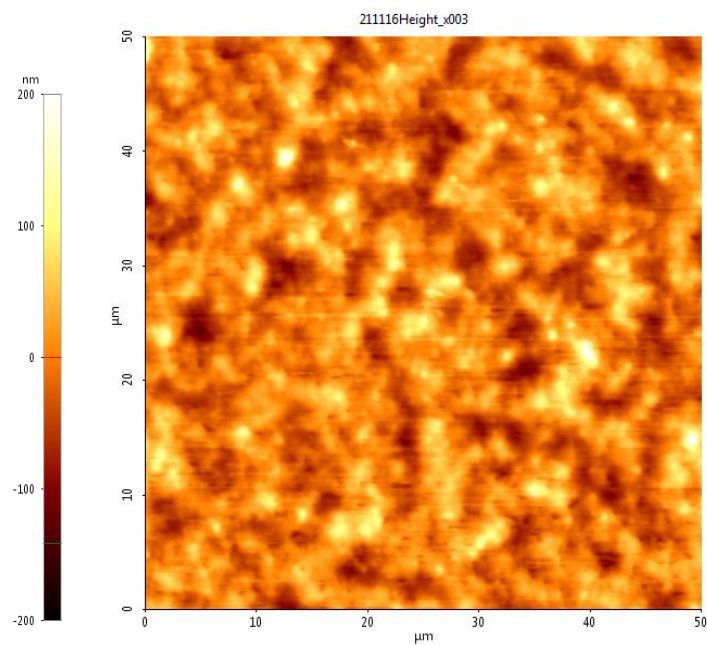


Fig. S19: AFM images of  $N = 5$  layers of (a) pristine M-PMA and (b) M-PGNP transferred on Silicon. The presence of pinholes in M-PMA layer is clearly visible.

The consequence of the presence of pinholes in PMA layers can be seen in the  $J_w$  and  $R_S$

histograms shown in Fig. S20. Although, overall  $J_w$  values are higher compared to PGNP layers with similar value of  $N$ , the  $R_S$  values are very poor leading to these being ineffective as separation membranes.

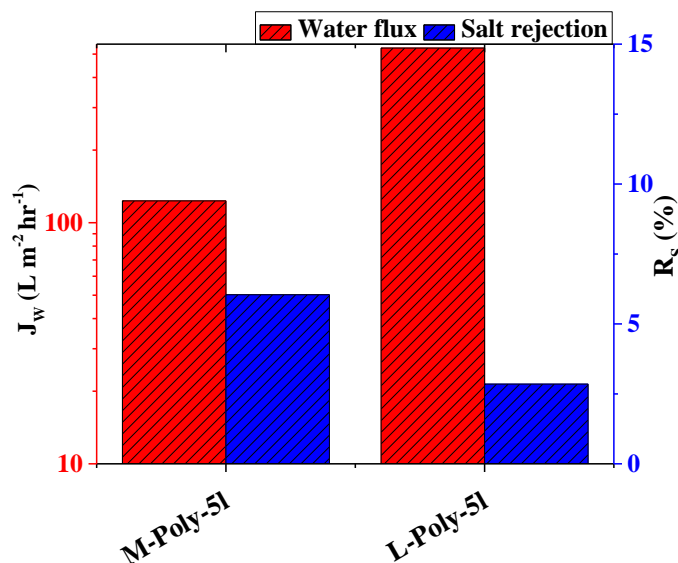


Fig. S20:  $J_w$  and  $R_S$  for pure polymer based membranes with  $N=5$  transferred on modified PA membranes. Although  $J_w$  values are higher compared to corresponding PGNP membranes the  $R_S$  values are significantly lower and not suitable as high-quality separation membranes.

## References

- (1) Jhalaria, M. Accelerated local dynamics in matrix-free polymer grafted nanoparticles. *Physical review letters* **2019**, *123*, 158003.
- (2) Shi, M.; Wang, Z.; Zhao, S.; Wang, J.; Wang, S. A support surface pore structure reconstruction method to enhance the flux of TFC RO membrane. *Journal of membrane science* **2017**, *541*, 39–52.
- (3) Masselin, I.; Durand-Bourlier, L.; Laine, J.-M.; Sizaret, P.-Y.; Chasseray, X.; Lemordant, D. Membrane characterization using microscopic image analysis. *Journal of Membrane science* **2001**, *186*, 85–96.

- (4) Swain, A.; Das, N. A.; Chandran, S.; Basu, J. K. Kinetics of High Density Functional Polymer Nanocomposite formation by Tuning Enthalpic and Entropic Barriers. *Soft Matter* **2022**,
- (5) Das, A.; Swain, A.; Begam, N.; Bhattacharyya, A.; Basu, J. Temperature-Driven Grafted Nanoparticle Penetration into Polymer Melt: Role of Enthalpic and Entropic Interactions. *Macromolecules* **2020**, *53*, 8674–8682.
- (6) Das, N. Thermal stability and dynamics of soft nanoparticle membranes: role of entropy, enthalpy and membrane compressibility. *Soft matter* **2020**, *16*, 1117–1124.
- (7) Yan, H.; Miao, X.; Xu, J.; Pan, G.; Zhang, Y.; Shi, Y.; Guo, M.; Liu, Y. The porous structure of the fully-aromatic polyamide film in reverse osmosis membranes. *Journal of Membrane Science* **2015**, *475*, 504–510.